TU Delft

Delft University of Technology

Metal Hydride Based Optical Hydrogen Sensors

Bannenberg, L.J.; Boelsma, C.; Asano, Kohta; Schreuders, H.; Dam, B.

DOI
10.7566/JPSJ.89.051003

Publication date
2020

Document Version
Final published version

Published in
Journal of the Physical Society of Japan

Citation (APA)
Bannenberg, L. J., Boelsma, C., Asano, K., Schreuders, H., & Dam, B. (2020). Metal Hydride Based Optical Hydrogen Sensors. *Journal of the Physical Society of Japan*, *89*(5), 051003-1-051003-9. Article 051003. https://doi.org/10.7566/JPSJ.89.051003

Important note
To cite this publication, please use the final published version (if applicable).
Please check the document version above.

Copyright
Other than for strictly personal use, it is not permitted to download, forward or distribute the text or part of it, without the consent of the author(s) and/or copyright holder(s), unless the work is under an open content license such as Creative Commons.

Takedown policy
Please contact us and provide details if you believe this document breaches copyrights.
We will remove access to the work immediately and investigate your claim.

This work is downloaded from Delft University of Technology.
For technical reasons the number of authors shown on this cover page is limited to a maximum of 10.

J. Phys. Soc. Jpn.
Downloaded from journals.jps.jp by 82.161.147.56 on 11/03/20

Journal of the Physical Society of Japan **89**, 051003 (2020)
https://doi.org/10.7566/JPSJ.89.051003

Metal Hydride Based Optical Hydrogen Sensors

Lars J. Bannenberg[1]*, Christiaan Boelsma[1], Kohta Asano[2], Herman Schreuders[1], and Bernard Dam[1†]

[1]*Materials for Energy Conversion and Storage (MECS), Department of Chemical Engineering, Delft University of Technology, P. O. Box 5045, Delft 2600 GA, The Netherlands*
[2]*Research Institute of Energy Frontier, National Institute of Advanced Industrial Science and Technology (AIST), Tsukuba, Ibaraki 305-8569, Japan*

(Received October 9, 2019; accepted December 20, 2019; published online February 25, 2020)

Hydrogen is playing a key role in the transition to a sustainable economy and in a variety of industrial processes. For its safe handling, the detection of hydrogen in a fast, reliable and accurate manner is crucial. Thin film metal hydride based optical hydrogen sensors provide an attractive option to sense hydrogen in a variety of conditions and have an attractive safety benefit over other methods of detection: They do not require the presence of electrical leads near the sensing area. These sensors rely on a change of the optical properties arising from a change in the hydrogenation of the metal hydride sensing layer in response to a different partial hydrogen pressure in the environment of the sensor. In this paper, we review how the performance and characteristics of an optical hydrogen sensor are related to the material properties of the metal hydride sensing layer and we discuss previously considered materials and challenges and opportunities left for the future.

1. Introduction

The transition to a sustainable energy system requires an increasing role for hydrogen as a transportation fuel, storage medium, and as a feedstock for the chemical industry.[1,2] As hydrogen is highly explosive in air, any leakage should be detected well before the explosive limit of about 4% is reached. Furthermore, the monitoring of the hydrogen concentration and pressure in a gas grid or in hydrogen storage systems is vital for its operation. Therefore, reliable hydrogen sensors are required to sense hydrogen accurately and hysteresis-free over a wide range of partial pressures and in a variety of chemical environments and gas mixtures (see, e.g., Refs. 3–6 for recent reviews).

At present, the detection of hydrogen is mainly carried out using catalytic resistor detectors or electrochemical devices. These systems are relatively large and expensive, require regular calibration and the presence of oxygen. Moreover, the current leads are a possible explosion hazard. For the automotive industry, sensors based on changes in the thermal conductivity were developed. Although these sensors do not require the presence of oxygen, they have the major drawback that they can only operate in a limited pressure range.[3,7,8]

Alternatively, optical changes occurring upon hydrogenation of some metals allow for the development of optical fiber based hydrogen sensors. The principle behind these sensors is simple: a change in the partial hydrogen pressure emanates in a change of the hydrogenation of the metal hydride, which in turn changes the dielectric function and thus the optical properties of the metal hydride sensing layer. As such, these sensors benefit from the fact that they do not require the presence of electrical leads in the area of measurement.[5,6,9–15]

In the past decades, hydrogen detection schemes have been developed for metal hydrides using either intensity modulation or frequency shifts in the optical transducer. In principle, the latter type, which makes for example use of a shift of the Localized Surface Resonance Peak[16–18] or wavelength modulation using fiber Bragg gratings,[15,19] is more reliable since this type of sensor is insensitive to intensity fluctuations of the light source. Moreover, the contrast/resolution is largely decoupled from the amount of material used, which allows one to limit the absolute amount of hydrogen absorbed such that shorter response times can be achieved. However, the implementation of such devices is typically more complex and cost-intensive as compared to sensors based on intensity modulation, which sometimes can even be read by the naked eye (Fig. 1). In the latter case, one makes use of the change in color obtained on hydrogenation, which is enhanced by making use of properly designed interference effects.[20]

More common is to measure the change in reflection of a metal hydride deposited at the top of an optical fiber. In such a micro-mirror configuration (Fig. 2), modulated light is guided through an optical fiber and reflected by the metal hydride sensing layer deposited at the top of the fiber. The intensity of the reflected light is monitored by a photodetector.[11,12] The signal obtained corresponds to the equilibrium between the ambient hydrogen pressure and the hydrogen absorbed by the metal: The amount of hydrogen absorbed is determined by the thermodynamics, while the resulting changes in the dielectric function give rise to the contrast in the optical signal.

In this paper, our focus is on the behavior of metal hydride based optical hydrogen sensors having a continuous thin film geometry and using intensity modulation as a readout. While also materials such as WO_3 have been considered for hydrogen sensing applications,[15,21] we restrict ourselves here to metal hydrides and formulate design rules for their use in such devices. Nevertheless, the principles and physics we discuss to choose the appropriate material are largely applicable to all types of optical metal hydride based hydrogen sensors and highly relevant to metal hydride based sensors based on changes in the electric resistivity.[3]

2. Metal Hydride Basics

The absorption of hydrogen by a metal depends on the temperature and gas pressure and is described by the Pressure–Concentration–Isotherm (PCI) of which an example is provided, together with the archetype metal-hydride phase diagram, in Fig. 3(a). Typically, at low hydrogen pressures P_{H2}, hydrogen is present in a diluted solid solution with a

©2020 The Physical Society of Japan

J. Phys. Soc. Jpn.
Downloaded from journals.jps.jp by 82.161.147.56 on 11/03/20

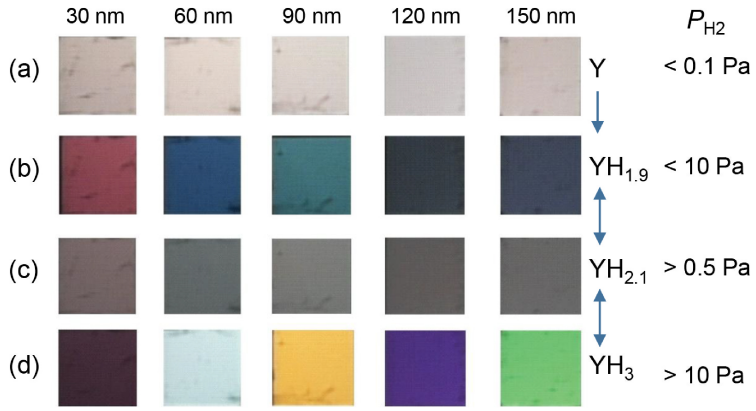

Fig. 1. (Color online) Apparent colors of a Pd capped Y film deposited on and viewed through a quartz substrate showing the effect of the Y thickness on the observed color at the different hydrogenation states. In the as-prepared state (a) the film has never experienced a pressure large than $P_{H2} = 0.5$ Pa. When the pressure exceeds this value the dihydride $YH_{2.1}$ state (c) is obtained, while for $P_{H2} > 10$ Pa the trihydride YH_3 state (d) is found. Note, that after exposure to $P_{H2} > 10$ Pa, Y dehydrogenates under normal conditions to the $YH_{1.9}$ state. However, due to the hysteresis, this color is only obtained when the partial hydrogen pressure is well below $P_{H2} = 0.5$ Pa. The Pd capping layer is 50 nm thick, i.e., much thicker than usual (5–10 nm), to enhance the interference effect. Pictures were made at room temperature using a 50 W halogen lamp light source and a Sony 3CCD camera. This figure is reproduced from Ref. 20 with modifications. © 2013 WILEY-VCH Verlag GmbH & Co. KGaA, Weinheim.

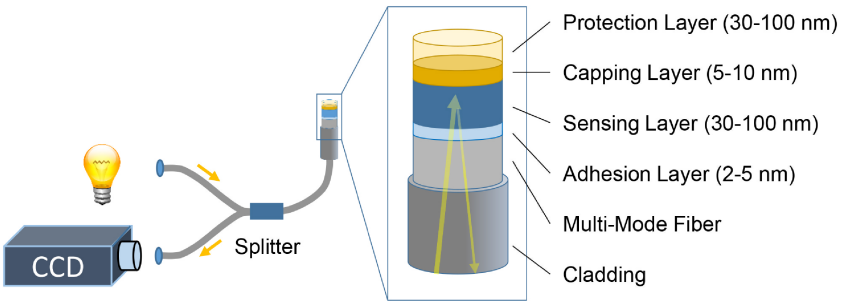

Fig. 2. (Color online) Schematic representation of a micro-mirror optical hydrogen sensor. The light, originating from the light source, is coupled into the fiber and transported to the tip of the optical fiber sensor. The light is partially reflected by the layer stack deposited on the tip of the fiber (see inset) and then passed back through the fiber and the splitter. The signal is subsequently measured by a photodetector as, e.g., a charge-coupled device (CCD). Upon a change in hydrogen pressure, the hydrogenation of the sensing layer (30–100 nm) changes, which in turn results in a change of the optical properties and thus the amount of light reflected by the layer stack and detected by a photodetector. The sensing layer is cleaved to the substrate by a 3–5 nm adhesion layer that is often made of Ti. A capping layer (typically Pd or a Pd-based alloy) is used to prevent oxidation of the sensing layer and to catalyze the hydrogen adsorption. This 5–10 nm capping layer is coated with protective polymeric layers as, e.g., PTFE and PMMA to protect the Pd layer from being poisoned by harmful chemical species and to further enhance the kinetics of the sensor. Some hydrogen sensors integrate the sensing and capping layer by using a Pd-based alloy (see Sect. 3). The figure is not to scale.

relatively small hydrogen-to-metal ratio H/M, the so-called α-phase. As the pressure increases, hydrogen continues to be absorbed until elastic H–H interactions become dominant and a β-hydride phase starts to nucleate. The subsequent growth of the β-phase occurs at a constant pressure at the expense of the α-phase. This first order phase transition is observed as a plateau in the PCI diagram. When all of the α-phase is transformed into the β-phase, the pressure rises again with a continuous increase of the hydrogen content in the β-phase. The hydrogen pressure at which the $\alpha \rightarrow \beta$ phase transformation takes place, is called the plateau pressure p_{plat}. The plateau disappears completely above the critical temperature T_C where the α-phase exists as an extended solid solution phase. While the above description is valid for a wide range of metal hydrides such as the archetype metal hydride Pd and frequently studied Mg, other metals such as Ti, Hf, and Ta exhibit more complex phase diagrams that include additional phases (see Sect. 5).

The first order $\alpha \rightarrow \beta$ phase transition can be used to design hydrogen threshold detectors. These detectors take advantage of the abrupt change in the optical transmission at the plateau pressure of the coexistence region owing to the sudden increase of H/M. However, a sizable hysteresis of the plateau pressure must be taken into account. For sensor applications it is typically preferred to keep the metal in a single phase as it allows the design of a device in which the optical signal changes continuously and hysteresis-free with pressure.

The readout of metal hydride based sensors and detectors depends on temperature. In general, at higher temperatures less hydrogen is absorbed. This implies that the temperature of a metal hydride based sensor needs to be monitored to compensate for the temperature dependence of p_{plat} (threshold detector) or the equilibrium pressure p_{eq} (sensor). The temperature dependence of p_{plat} in a threshold detector is given by Van 't Hoff's equation:

$$\ln \frac{p_{eq}}{p_0} = \frac{\Delta H}{RT} - \frac{\Delta S_0}{R}, \quad (1)$$

where p_0 is the standard pressure, R the gas constant, T the absolute temperature and ΔH and ΔS_0 are the enthalpy

©2020 The Physical Society of Japan

J. Phys. Soc. Jpn.
Downloaded from journals.jps.jp by 82.161.147.56 on 11/03/20

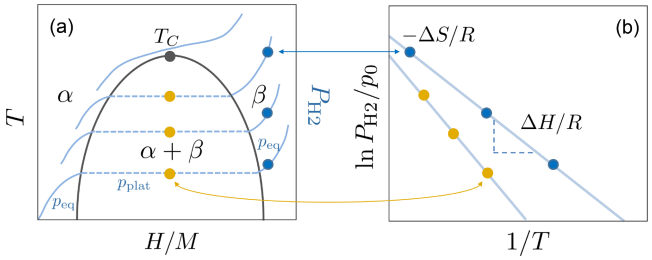

Fig. 3. (Color online) Temperature T and hydrogen-to-metal H/M ratio phase diagram of a typical metal hydride and examples of PCIs. The α-phase is a diluted solid solution in which hydrogen is typically present in low concentrations. The β-phase is the high hydrogen concentration hydride phase that coexists at intermediate H/M with the α-phase. Above the critical temperature T_C, no phase-coexistence (and corresponding first-order phase transition) occurs and only a α-phase exists as an extended solid solution phase. The blue lines and the right axis indicate PCIs. At low and high H/M, the equilibrium pressure p_{eq} is at a given temperature monotonically increasing in H/M. In the region of phase coexistence, a plateau is seen at the plateau pressure p_{plat}, which shifts with increasing temperature to higher pressures. (b) Example of a Van 't Hoff plot that can be used to obtain the enthalpy ΔH and entropy ΔS_0. By plotting the natural logarithm of the normalized equilibrium pressure at a given H/M ratio as a function of the inverse temperature, ΔH and ΔS_0 may, according to Van 't Hoffs equation [Eq. (1)], be obtained from the slope and intercept of a linear fit through the points, respectively.

(kJ mol_{H2}^{-1}) and entropy (J K^{-1} mol_{H2}^{-1}) of the hydrogenation reaction, respectively. For most metal hydrides, the entropy change is mainly determined by the loss of entropy when the gaseous H_2 molecule is dissociated and adsorbed by the metal, i.e. $\Delta S_0 = \Delta S_{H2} = 130.7\,\mathrm{J\,K^{-1}\,mol_{H2}^{-1}}$. However, vibrational and configurational entropy differences between the solid α and β phases do play a role, as shown by the value measured in Pd: $\Delta S_0 \cong -94\,\mathrm{J\,K^{-1}\,mol_{H2}^{-1}}$.[22] In general, in a solid solution, the behavior of the enthalpy and entropy as a function of the hydrogen concentration is only phenomenologically understood.

To select a proper sensing material, one may search for the thermodynamic data collected on bulk powders. These enthalpy and entropy values are usually quoted far above room temperature. To calculate p_{eq} at lower temperatures one uses the Van 't Hoff equation. As illustrated by Fig. 3(b), by extrapolating the logarithm of the equilibrium pressure as a function of the inverse temperature, the enthalpy and entropy of the hydride formation are calculated and the low temperature equilibrium plateau pressure may be obtained. This method also applies to solid solutions, where the hydrogen content is a monotonically increasing function of the pressure. In this case, one needs to make sure that the p_{eq}'s at different temperatures are measured at exactly the same H/M ratio. These hydrogen concentrations can be found through, e.g., nuclear reaction analysis[23] or neutron reflectometry.[24]

3. Design of the Hydrogen Sensor

As shown in Fig. 2, optical hydrogen sensors are typically composed of several metal hydride layers. These metal hydride films are usually obtained by sputtering or evaporation of the corresponding metal. The first and most frequently considered sensing material is Pd and alloys thereof. Besides absorbing hydrogen without the need of a catalyst, Pd has a variety of attractive hydrogen sensing properties: it offers a relatively large optical contrast over a modest sensing range of partial hydrogen pressures of $P_{H2} = 10^{+1}$–10^{+4} Pa at room temperature with response times that can be in the order of seconds. However, its applicability is limited by the substantial hysteresis originating from the first order transition from dilute α-PdH_x to the higher concentration PdH_x β-phase. Therefore, alloying has frequently been employed to lower T_C and suppress the first order transition in order to obtain reproducible sensing characteristics (see Sect. 5.1).

A wider range of sensing materials can be obtained by applying Pd-based capping layers on top of another metal hydride and in this way separate the hydrogen sensing and dissociation functionality. In such sensors, the Pd layer takes care of the hydrogen dissociation and the bottom sensing layer mainly determines the optical sensing properties. In this case, the Pd layer does not only catalyze the hydrogen (de)sorption of the sensing layer but also acts as a selector, preventing deactivation of the sensor by, e.g., the oxidation of the sensing layer. Based on experience, sufficient protection is already provided by a relatively thin (5–10 nm) Pd layer.

A problem with Pd-capped sensors is the limited hydrogen solubility at relatively low hydrogen pressures which causes long response times. To combat this, Pd-capped hydrogen sensors are typically operated at increased temperatures (typically 90–150 °C) where the hydrogen mobility is substantially larger than at room temperature. Alternatively, one may increase the hydrogen solubility at low hydrogen pressures by alloying the Pd capping layer with elements like Au, Ag, and Ta and in this way promote the (de)sorption kinetics.

The catalytic Pd surfaces are prone to poisoning by humidity and chemical species such as NO_x and CO, all omnipresent in atmospheric conditions.[25–28] To improve the reproducibility of the signal in realistic sensing environments, protection layers are needed to keep the Pd surface active. Polytetrafluoroethylene (PTFE) effectively reduces the poisonous effect of humid air. Interestingly, as shown in Fig. 4, PTFE also positively affects the kinetics of the absorption and desorption processes process.[26,27,29] For this effect both electrostatic and surface catalytic effects were proposed.[26] Another well-known poisonous adsorbent is CO for which a combination of PTFE and poly(methylmethacrylate) (PMMA) was developed as a protection layer.[27] In fact, such polymeric capping layers allow for the application of optical hydrogen sensors in oily liquids such as employed in high-voltages transformers.[30] Furthermore, protection against deactivating chemical species can also be achieved by alloying the Pd capping layer (or alloys of Pd) with suitable elements as, e.g., Cu to prevent CO poisoning.[28]

In the past, Pd-based sensors had a limited cycle lifetime. Due to hydrogenation, thin films may expand up to 30% in volume resulting in delamination of the film upon repeated cycling.[31,32] To prevent this, 2–5 nm thick intermediate layers are used to improve the attachment to the support. Titanium, which is under normal conditions immiscible with Pd, was found to stabilize the sensing layers leading to a stability of over hundreds of cycles.[29,33–35] While delamination is prevented in this way, the confinement of the film to the substrate results in stress and plastic deformation upon

©2020 The Physical Society of Japan

J. Phys. Soc. Jpn.
Downloaded from journals.jps.jp by 82.161.147.56 on 11/03/20

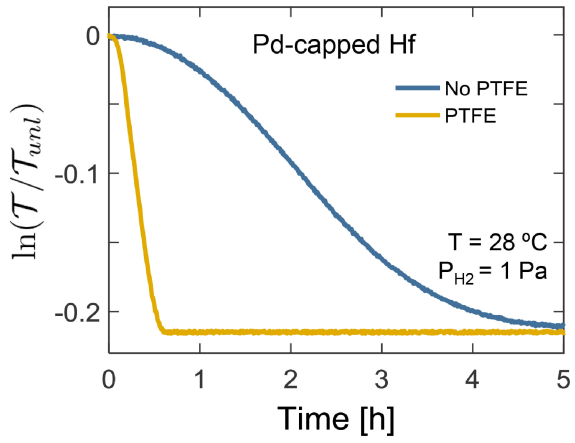

Fig. 4. (Color online) Effect of sputtered PTFE on the kinetic properties of two 40 nm Hf thin films capped with a 10 nm Pd layer with and without an additional PTFE layer. The two films were simultaneously exposed to a constant hydrogen pressure of $P_{H2} = 1$ Pa at $T = 28$ °C. The white-light optical transmission $\mathcal{T}$ is normalized to the transmission of the unloaded states $\mathcal{T}_{unl}$. Data adapted from Boelsma et al. (2017).[29]

hydrogenation of the layer.[32,35–40] Both effects induce deviations from the expected equilibrium plateau pressure and the hysteresis therein. Interestingly, the amount of plastic deformation is less in nano-structured thin films. On the other hand, in continuous films, stress may increase the critical temperature which favors a hysteresis-free behavior.[35,39,41] However, the plastic deformation of the film upon hydrogenation may also be a source of hysteresis.[32,35,39]

4. Finding the Right Sensing Material

Although optical hydrogen sensors typically make use of changes of the optical reflectivity of a sensing layer (see Fig. 2), most experimental studies in the field of optical hydrogen sensors have been performed by measuring the optical transmission. The reason for this is simple: measuring the optical transmission in, e.g., a hydrogenography set-up[42] is in general much more practical and also allows one to evaluate the thermodynamics and kinetics of potential hydrogen sensing materials. Importantly, the changes in optical transmission provide information about the responses of the dielectric function to changes in hydrogenation. Data and knowledge about this is scarce, making it difficult to a priori predict and select materials with a suitable optical contrast. An additional advantage of optical transmission studies is the possibility to measure a large number of samples simultaneously or to investigate the optical transmission over large area films with controlled composition and/or thickness gradients. Such gradients can be created by co-deposition from two, three or more off-centered metal sources.[42] These techniques facilitate the identification of the most suitable composition and layer thickness for sensing applications in a matter of days. It is important to note that optical transmission methods are not confined to materials showing a metal–insulator transition on hydrogenation: metals such as Pd and Hf can be studied in transmission as long as the layer is sufficiently thin (<100 nm).

When using optical transmission measurements, knowledge of the relation between the optical transmission and the hydrogen content is vital to be able to understand the thermodynamics of the sensing material. Lambert's Law relates the transmittance $\mathcal{T}$ of a sensing material, i.e., the ratio of the transmitted intensity (or radiant flux) I to the initial intensity I_0, to the wavelength-dependent attenuation coefficient $\mu(x,\lambda)$ and thickness of the sensing layer z. In its most basic form, it can be written as:

$$\mathcal{T}(x,\lambda,z) = \frac{I(z)}{I_0} = e^{-\mu(x,\lambda)z}, \tag{2}$$

where we assume that the attenuation coefficient $\mu(x,\lambda)$ is uniform across the thickness of the sensing layer.

For a two phase system with limiting compositions x_1 and x_2 the optical signal is determined by the attenuation coefficient of the low-hydrogen concentration α-phase $\mu_1(x,\lambda)$ and the attenuation coefficient of the high hydrogen concentration β-phase $\mu_2(x,\lambda)$. In accordance with Beer's law, the attenuation coefficient of the two-phase material equals:

$$\mu(x,\lambda) = (1-f)\mu_1(x,\lambda) + f\mu_2(x,\lambda), \tag{3}$$

where f is the fraction of the high hydrogen concentration phase. Substituting Eq. (3) in Eq. (2) and using $f = (x - x_1)/(x_2 - x_1) = \Delta x/(x_2 - x_1)$, one obtains:

$$\mathcal{T}(x,\lambda,z) = e^{-\mu_1(x_1,\lambda)z} e^{-z(\mu_2(x_2,\lambda)-\mu_1(x_1,\lambda))\frac{\Delta x}{x_2-x_1}}. \tag{4}$$

Recognizing that $\mathcal{T}_0 = e^{-\mu_1(x_1,\lambda)z}$ is the transmission of the α-phase, one can rewrite Eq. (3) as:

$$\ln\left(\frac{\mathcal{T}(x,\lambda,z)}{\mathcal{T}_0}\right) = -(\mu_2(x_2,\lambda) - \mu_1(x_1,\lambda))\frac{\Delta x}{x_2 - x_1} z$$
$$= -c(\lambda)\Delta x z, \tag{5}$$

where $c(\lambda)$ is a wavelength-dependent constant.

Equation (5) is a surprisingly simple result: it shows that there is a linear relationship between the change in hydrogen content of the sensing layer and $\ln(\frac{\mathcal{T}(z)}{\mathcal{T}_0})$ for a two phase system. This result only holds provided that the two phases are randomly distributed, have a constant hydrogen content (e.g., the total hydrogen content may only vary as a result of changing phase fractions and not as a result of different hydrogen content of the two phases itself or the distribution of the two phases), and the size of the domains is reasonably small.

Besides to two-phase systems, Eq. (5) has been widely applied to solid solutions, albeit strictly speaking not valid for the absorption of hydrogen within one phase. In fact, Eq. (5) only holds when the effect on the attenuation coefficient of hydrogen sorption is independent of the hydrogen concentration within the metallic host.

Although this sounds like a rather crude assumption, the empirical results for one phase systems show indeed often a linearity.[29,35,43–45] Figure 5 depicts the relation between the hydrogen content as a function of the white-light optical transmittance for three hydrogen sensing materials with a large solubility range within one phase: Pd-capped Hf and Ta[29,43] as well as $Pd_{0.7}Au_{0.3}$.[35] These materials all show a linear dependence of the transmission on the hydrogen content, either in a positive (e.g., Pd) or a negative (e.g., Hf and Ta) sense.

The fact that the linearity holds over such a large range of hydrogen contents is most surprising. It calls for a more advanced approach including an experimental and computational study of the dielectric functions of metal hydrides for

©2020 The Physical Society of Japan

J. Phys. Soc. Jpn.
Downloaded from journals.jps.jp by 82.161.147.56 on 11/03/20

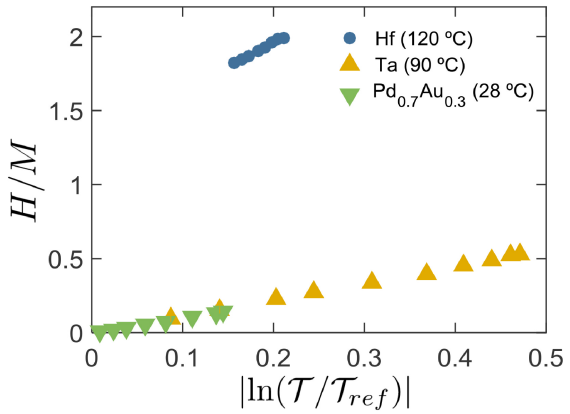

Fig. 5. (Color online) The hydrogen-to-metal ratio H/M as a function of the optical contrast for a Pd-capped 40 nm Hf thin film (120 °C), a Pd-capped 40 nm Ta thin film with a 4 nm Ti adhesion layer (90 °C) and a 40 nm $Pd_{0.7}Au_{0.3}$ thin film with a 4 nm Ti adhesion layer (28 °C). The change of the white light optical transmission $\mathcal{T}$ was measured relative to the unloaded state for Hf and the as prepared state for Ta and $Pd_{0.7}Au_{0.3}$. Data adapted from Bannenberg et al. (2019).[43)]

various hydrogenations and a complete modeling of the thin-film systems. Efforts have already been made in this direction. Particularly noteworthy are the experimental results reported in Refs. 46 and 47, which indeed indicate for various metal hydrides a linear dependence of the real and imaginary component of the dielectric constant over a wide wavelength and hydrogen content range.

5. Rational Choice of Sensing Materials

In this paper, we focused on the material properties of metal hydrides in relation to the optical hydrogen sensor's performance and functionality with the overall aim to develop a hysteresis-free sensor that responds to a hydrogen pressure in a quick and reliable way over a wide pressure range and in a variety of chemical environments. Table I relates these desired properties to material properties of a metal hydride and other design choices. From this table, it becomes apparent that although, e.g., a strong dependence of the dielectric function on the hydrogen content improves the resolution without compromising other characteristics, other properties are strongly interrelated. For example, a small increase of the hydrogen content with a changing hydrogen pressure is desired to obtain a large sensing range, which at the same time compromises the resolution with which one can determine the hydrogen pressure. As a result a one-size-fits-all hydrogen sensor is probably not possible and tailor-made sensing solutions need to be developed.

Generally speaking, two approaches have been used to develop these hydrogen sensors with desirable properties: (i) materials in which the hydrogen dissociation and optical response are integrated as, e.g., (alloys) of Pd and (ii) materials that separate the hydrogen dissociation functionality from the optical response as, e.g., Pd capped transition metals. We provide examples of both approaches below and discuss how certain materials were rationally chosen and altered to improve the performance of the hydrogen sensor.

5.1 Hydrogen sensors with integrated hydrogen sensing and dissociation functionality

The first and most frequently considered material for hydrogen sensors is Pd as it can readily absorb hydrogen at room temperature without the need of a catalyst and its resistance to oxidation (see Sect. 3). It has a set of attractive sensing properties, including a relatively large optical contrast and a modest sensing range of $P_{H2} = 10^{+1}$–10^{+4} Pa at room temperature and response times that can be in the order of seconds. However, its applicability is limited by the considerable hysteresis resulting from the first-order transition from the dilute α-PdH_x to the higher concentration PdH_x β-phase, that can only be avoided by increasing the operating temperature beyond $T_C \approx 290$ °C, which is impractical for most applications.

Alloying of Pd has often been employed to lower T_C and suppress the first order transition. Most frequently, Pd alloys with Au,[33–35,48)] Ag,[49)] Cu,[28)] and Ta[50)] were considered. The sensing characteristics of these materials are largely similar: As exemplified in Fig. 6 for the case of $Pd_{1-y}Ta_y$, increasing the concentration of the dopant decreases the critical temperature, and, for high enough concentrations, the first-order transition is completely suppressed and the unwanted hysteresis is (largely) eliminated. In addition, the doping of Pd by these elements typically results in a larger unit cell, which enables hydrogenation at lower hydrogen pressures, thereby extending the sensing range to lower pressures. In the case of $Pd_{1-y}Au_y$, an impressive sensing range of at least $P_{H2} = 10^{0}$–10^{+6} Pa at room temperature has been demonstrated,[35)] and this range likely extends to even higher pressures, making it so far the material of choice to probe relatively high hydrogen pressures. However, the enlarged sensing range and reduced hysteresis come at the cost of a

Table I. List of desirable properties of metal hydride based optical hydrogen sensors and how these can be achieved.

Desirable property	How to achieve?
Large sensing range	Large solubility range within one phase and/or within multiple phases with a coherent phase transition. Small dx/dP_{H2} (large slope in pressure composition isotherm)
Large optical contrast	Large dx/dP_{H2} Large change of dielectric function with changing hydrogen content Take a wavelength where optical changes are the largest
No hysteresis	No first-order phase transition No stress-induced hysteresis/plastic deformation
Fast response time	Select materials with a high hydrogen diffusion constant Low volumetric expansion Thin sensing layer Small dx/dP_{H2} Apply surface coatings to lower activation energy
Suitable operating temperature	Appropriate ΔH and ΔS
High stability	Select materials not sensitive to oxidation Low volumetric expansion Good adhesion between sensing layer and support
Resistant to other chemical species	Apply protective coatings (e.g., PTFE/PMMA) Introduce dopants in capping layers as e.g., Cu in Pd to prevent deactivation by CO

©2020 The Physical Society of Japan

J. Phys. Soc. Jpn.
Downloaded from journals.jps.jp by 82.161.147.56 on 11/03/20

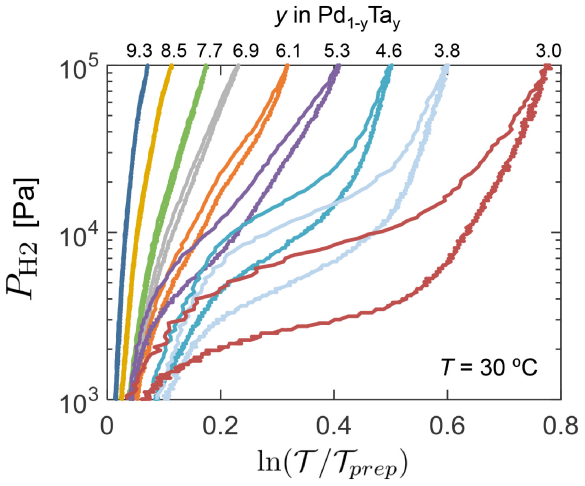

Fig. 6. (Color online) Pressure-Transmission-Isotherms (PTIs) of $Pd_{1-y}Ta_y$ films measured at $T = 30\,°C$ during the fifth hydrogen absorption and desorption cycle. The white-light transmission $\mathcal{T}$ was measured relative to that of the as-prepared film $\mathcal{T}_{prep}$. For lower Ta concentrations hysteresis between hydrogen absorption and desorption is observed whereas at higher Ta concentrations the hysteresis disappears. The concentration of Ta in the alloy (at. %) is indicated at the top of the corresponding isotherms. Data adapted from Westerwaal et al. (2012).[50)]

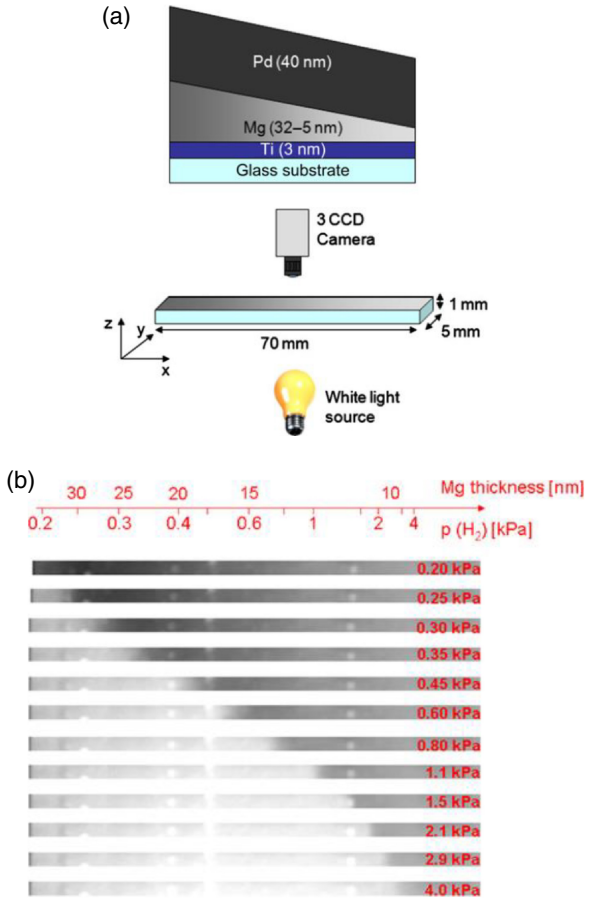

Fig. 7. (Color online) (a) Design of an eye-readable hydrogen sensor based on a Pd-capped Mg thin film with a varying Mg thickness. The sample consist of a wedge of Mg with varying thickness along the *x*-direction. The Mg wedge is sandwiched between a 40 nm Pd-capping layer and a 3 nm Ti-adhesion layer deposited on a $70 \times 5 \times 1\,mm^3$ glass substrate. The white light optical transmission is measured with a 3CCD camera. (b) Images of the sample when it was exposed to different increasing partial hydrogen pressures of $P_{H2} = 12$–$4{,}000\,Pa$ at room temperature. Mg has a metal-to-insulator transition when it hydrogenates to MgH_2, thus becoming highly transparent upon hydrogenation. The sensor makes use of the profound thickness dependence of the plateau pressure of Mg thin films, which ensures that the metal-to-insulator transition occurs at different pressures. The Mg layer thickness and hydrogenation pressure are reported at the top. This figure is reproduced from Ref. 53 with modifications. © 2010 Elsevier.

substantially reduced optical contrast originating from the reduced hydrogen content of the sensing layer. Moreover, a small hysteresis can still be discerned as a result of stress-induced effects arising from the clamping of the film to the support. As such, the volumetric expansion of the cubic unit cell manifests itself as an increase of the thickness of the thin film. These effects can be avoided by using a discontinuous film geometry (e.g., arrays of nanoparticles deposited on a support) in which stress can be released as the unit cell can expand both in the in- and out-of-plane directions of the film.[35)]

5.2 *Hydrogen sensors with separate hydrogen sensing and dissociation functionality*

The efforts to develop hydrogen sensors with separate hydrogen sensing and dissociation functionality may roughly be divided into two classes of materials: (i) highly transparent Pd-capped metal hydrides such as Mg-based alloys and Y and (ii) Pd-capped transition metals such as Hf and Ta. The idea behind using Mg[42,51–55)] and Y[26,56,57)] is simple: both materials display a metal-to-insulator transition upon hydrogenation, which is accompanied by a profound change of their optical properties. As a result, a sensor can be developed with a high optical contrast, and potentially, a high sensitivity. Unfortunately, Mg has a phase diagram similar to the one shown in Fig. 3(a) and thus a substantial hysteresis is observed on (de-)hydrogenation. In addition, it is only sensitive to H_2 within a narrow pressure range around p_{plat} and thereby is best used as a hydrogen detector.

Alloying of Mg with, e.g., Ti, Ni, and Ni–Zr helps to increase the pressure range of the sensor.[42,51,52,54,55)] Although the Mg-based alloys typically exhibit a much larger sensing range than Mg, up to $P_{H2} = 10^{-1}$–$10^{+2}\,Pa$ for $Mg_{1-y-z}Ni_yZr_z$ at room temperature, they still have a sizable hysteresis.[54)] Alternatively, one may vary the layer thickness of a Pd-capped Mg film.[53)] Decreasing the thickness of Mg films lowers the enthalpy of hydrogenation significantly due to the increasing contribution of the interface energy.[58)] This effect has been exploited to create a Mg based sensor that is sensitive in a range from 12–4,000 Pa that can even be read by the bare eye (Fig. 7). However, Mg-based materials form extremely stable hydrides and thus exhibit slow desorption kinetics, typically only dehydrogenating in the presence of oxygen. Therefore, these sensors can in practice only be used as a single-use indicator of the highest hydrogen pressure that was present in the environment of the sensor. A similar eye-readable sensor was demonstrated by means of a composition gradient in Y-Zr thin films.[57)]

Another route to widen the scope of hydrogen sensing materials is to consider Pd-capped transition metals. By considering metals with a large hydrogen solubility within one phase, hysteresis arising from a first-order transition is simply circumvented. Tantalum is such a material: Above its modest critical temperature of $T_C = 61\,°C$ in bulk, a large solubility range exists within a distorted body centered cubic

©2020 The Physical Society of Japan

J. Phys. Soc. Jpn.
Downloaded from journals.jps.jp by 82.161.147.56 on 11/03/20

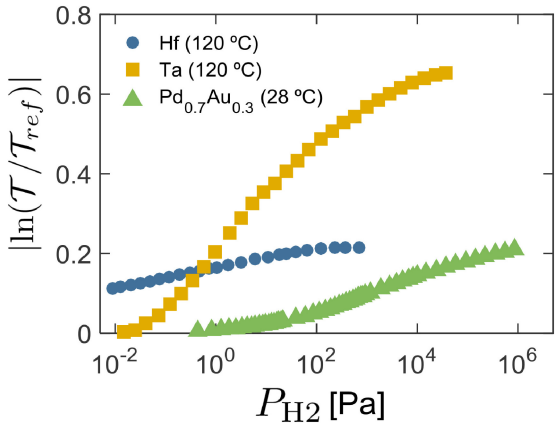

Fig. 8. (Color online) Comparison of the sensing range and optical contrast for a Pd-capped 40 nm Hf thin film (120 °C), a Pd-capped 40 nm Ta thin film with a 4 nm Ti adhesion layer (120 °C) and a 40 nm $Pd_{0.7}Au_{0.3}$ thin film with a 4 nm Ti adhesion layer (28 °C). The change of the white light optical transmission is measured relative to the unloaded state for Hf and the as prepared state for Ta and $Pd_{0.7}Au_{0.3}$. Note that the slope of the curves for Hf and Ta are inverted. Data adapted from Bannenberg et al. (2019).[43)]

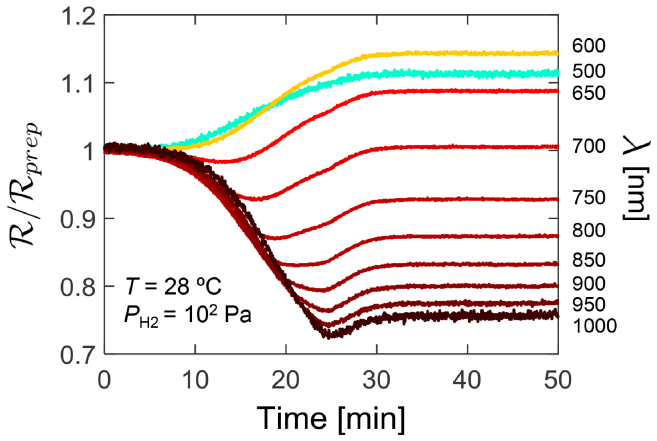

Fig. 9. (Color online) Wavelength dependence of the changes in reflectivity of a Pd-capped 40 nm Ta thin film with a 4 nm Ti adhesion layer. The thin film was exposed to a constant hydrogen pressure of $P_{H2} = 100$ Pa at room temperature. The reflectance $\mathcal{R}$ is measured relative to the reflectance of the as-prepared state $\mathcal{R}_{prep}$. Data adapted from Boelsma (2017).[55)]

phase that extends up to $TaH_{0.7}$.[43,59,60)] The sensing properties of Ta are indeed largely favorable: it enables a well-defined and reproducible optical signal that is free of hysteresis over an extensive sensing range of $P_{H2} = 10^{-2}$–10^{+4} Pa at 120 °C, making Ta especially well-suited for detecting relatively low hydrogen pressures (Fig. 8). The optical contrast is large as compared to, e.g., Pd-alloy hydrogen sensors (Fig. 8), allowing for the development of a high resolution hydrogen sensor. The large contrast is mainly due to the substantial change of x in TaH_x with a change of P_{H2}, i.e., a large value of dx/dP_{H2}. In fact, the contrast can be further optimized by selecting the wavelength at which the change in the optical properties is maximum (Fig. 9). However, the relatively large quantities of hydrogen that have to be dissociated and diffused through the film negatively influence the response time.

Hafnium is another example of a transition metal that has advantageous hydrogen sensing properties.[29,43)] Although at first sight the phase diagram makes Hf look rather unsuited for hydrogen sensing applications due to the first-order phase transitions (Fig. 10), Hf can be used to hysteresis-free detect hydrogen: Structural measurements of Hf show that the $\alpha \rightarrow \delta$ is irreversible under normal conditions, while the $\delta \rightarrow \epsilon$ transition is coherent in nature for thin films. The latter transition is included in the solubility range of $HfH_{1.4}$–$HfH_{2.0}$ in thin films in which a highly reproducible and hysteresis-free change in optical transmission in response to a hydrogen exposure is obtained over at least six orders of magnitude in pressure.

Special of Hf is the linear relationship between $\ln(\mathcal{T}/\mathcal{T}_0)$ or x in HfH_x, on the one side, and the logarithm of the pressure over at least six orders of magnitude in pressure, on the other side. It implies that the hydrogenation enthalpy ΔH is independent of x, while ΔS decreases linearly with increasing x to substantially negative values [see Eq. (1)]. Although the origin of this remarkable thermodynamic behavior is not yet understood, it is extremely useful for hydrogen sensing applications: a change in temperature uniformly shifts the optical signal to different pressures, facilitating an easy

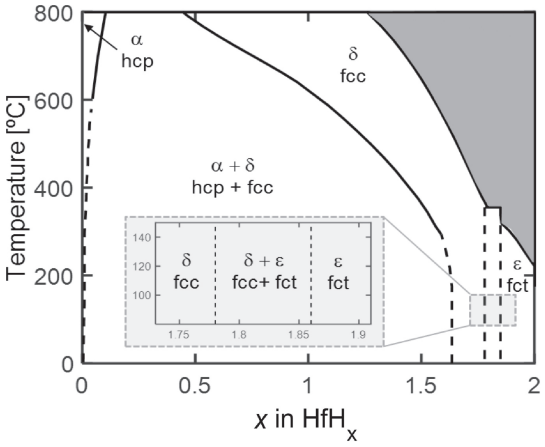

Fig. 10. Phase diagram for bulk hafnium-hydrogen after data from Mintz.[61)] α, δ, and ϵ indicate the hexagonal closed packed (hcp), face centered cubic (fcc), and face centered tetragonal (fct) phase. The shaded area indicates the region of the phase diagram where the hydride formation pressure exceeds 0.1 MPa in bulk. The inset shows a more detailed phase diagram for $1.72 \leq x \leq 1.92$. Although at first sight the phase diagram makes Hf look unsuited for hydrogen sensing applications due to the first-order phase transitions, Hf can be used to hysteresis-free detect hydrogen. The $\alpha \rightarrow \delta$ is irreversible under normal conditions and the $\delta \rightarrow \epsilon$ transition is coherent in nature for thin films. This figure is reproduced from Ref. 43 with modifications. © 2019 Elsevier.

calibration of the hydrogen sensor.[29)] Note, that the entropy values derived from the Van 't Hoff analysis yield values in the range between 180–240 $J\,K^{-1}\,mol_{H2}^{-1}$. This would counter-intuitively imply that in this compositional range the entropy of hydrogen in the solid is larger than that in the gas phase. The origin of this is not understood and cannot be derived from existing models of the configurational and vibrational entropy (see the supplement of Ref. 29). A recent analysis of Hf bulk powder at $T = 350$ °C (Fig. 11) reaffirms the original powder data,[61)] suggesting that the thin film nature of the Hf not only suppresses the fcc/fct transition, but in this case also has a profound influence on the thermodynamic behavior of this unique material.

©2020 The Physical Society of Japan

J. Phys. Soc. Jpn.
Downloaded from journals.jps.jp by 82.161.147.56 on 11/03/20

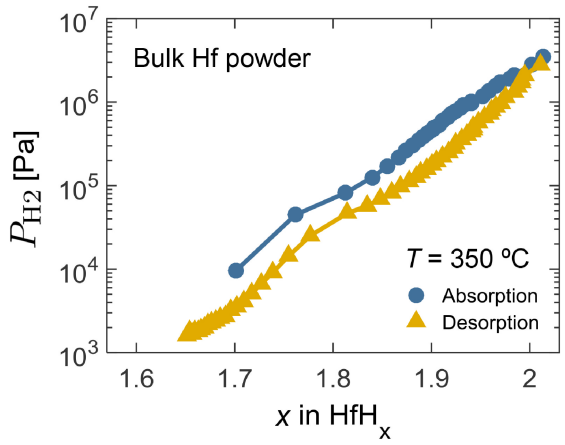

Fig. 11. (Color online) Pressure-Composition-Isotherm (PCI) of bulk powder Hf measured during the second exposure to hydrogen at $T = 350\,°C$. The 3.3 g Hf powder sample (sponge) was located inside a stainless steel tube which was first evacuated for 20 min. Subsequently, the pressure inside the tube was increased to $P_{H2} = 2$ MPa at $T = 350\,°C$ using hydrogen gas of 7N purity. Afterwards, the tube was evacuated for 3 h at $T = 650\,°C$ to dehydrogenate. The PCI was measured using the volumetric method.

The practical relevance of both Pd-capped Ta and Hf would be further enhanced when the operating temperature could be decreased to room temperature. Unfortunately, this results in extremely slow kinetics with response times in the order of hours (Fig. 4). In general, the kinetics of metal hydride hydrogen sensors is determined by the hydrogen dissociation at the Pd-capping layer, the transport of hydrogen within the capping layer, the transport across the capping-sensing layer interface and the transport within the sensing layer. Measurements of the diffusion of hydrogen through Ta indicate that the transport within the sensing layer is not the rate-limiting step.[43] On the other hand, the enhancement of the kinetics with a factor of about ten by coating the Pd-capping layer with PTFE (Fig. 4) shows that the dissociation of hydrogen at the surface plays an important role in the poor kinetics.[29] Furthermore, the transport through the Pd layer is slow as the hydrogen concentration is extremely low at low hydrogen pressures. Although the hydrogen concentration is even lower at elevated temperatures, the mobility of hydrogen is typically much lower at room temperature, resulting overall in improved kinetics at higher temperatures. To enhance the kinetics of the Hf- and Ta-based sensors, one could possibly increase the hydrogen concentration at low P_{H2} in the capping layer through doping with, e.g., Au, decrease the thickness of the sensing layers (i.e., decreasing the amount of hydrogen to be transported), and decrease the thickness of the capping layer (i.e., reducing the distance over which hydrogen needs to be transported). Furthermore, we note that room temperature results in a low hydrogen pressure sensing range for both Ta and Hf ($P_{H2} < 1$ Pa for Hf). Although this can be advantageous for certain applications, a sensitivity up to at least 4 kPa (i.e., the explosive limit of hydrogen in air at atmospheric pressure) is often beneficial when detecting potential hydrogen leaks. Although not yet unexplored, alloying of Hf and/or Ta could potentially shift the equilibrium pressure and, correspondingly, the sensing range to higher pressures.

6. Conclusion

In conclusion, over the past decades optical hydrogen sensors became attractive devices for reliably determining the hydrogen pressure, which is a prerequisite for a hydrogen based economy and in a variety of industrial processes. Although a one-size-fits-all hydrogen sensor is not likely to be developed, various compatible hydrogen sensors were proposed with each their distinguished advantageous and applications. We provided guidelines to further develop these tailor-made hydrogen sensors based on rationally selecting suitable materials and indicated directions and challenges for future research.

Acknowledgment The authors wish to acknowledge P. Ngene, M. Slaman, and R. Westerwaal for fruitful discussions and their contributions to the development of micro-mirror sensors within our group. The work of CB is financially supported by the Stichting voor Fundamenteel Onderzoek der Materie (FOM), which is financially supported by The Netherlands Organization for Scientific Research (NWO).

*l.j.bannenberg@tudelft.nl
†b.dam@tudelft.nl

1) A. Bakenne, W. Nuttall, and N. Kazantzis, Int. J. Hydrogen Energy **41**, 7744 (2016).
2) Hydrogen to the rescue: Nat. Mater. **17**, 565 (2018).
3) T. Hübert, L. Boon-Brett, G. Black, and U. Banach, Sens. Actuators B **157**, 329 (2011).
4) W. J. Buttner, M. B. Post, R. Burgess, and C. Rivkin, Int. J. Hydrogen Energy **36**, 2462 (2011).
5) C. Perrotton, N. Javahiraly, A. Kazemi, and P. Meyrueis, Proc. SPIE **8026**, 80260O (2011).
6) N. Javahiraly and C. Perrotton, Proc. SPIE **9202**, 920206 (2014).
7) I. Simon and M. Arndt, Sens. Actuators A **97–98**, 104 (2002).
8) L. Boon-Brett, J. Bousek, G. Black, P. Moretto, P. Castello, T. Hübert, and U. Banach, Int. J. Hydrogen Energy **35**, 373 (2010).
9) M. A. Butler, Appl. Phys. Lett. **45**, 1007 (1984).
10) R. C. Hughes, A. J. Ricco, M. A. Butler, and S. J. Martin, Science **254**, 74 (1991).
11) M. A. Butler, J. Electrochem. Soc. **138**, L46 (1991).
12) M. A. Butler, Sens. Actuators B **22**, 155 (1994).
13) M. Yang and J. Dai, Photonics Sens. **4**, 300 (2014).
14) S. F. Silva, L. Coelho, O. Frazão, J. L. Santos, and F. X. Malcata, IEEE Sens. J. **12**, 93 (2012).
15) Y. Zhang, H. Peng, X. Qian, Y. Zhang, G. An, and Y. Zhao, Sens. Actuators B **244**, 393 (2017).
16) C. Perrotton, R. J. Westerwaal, N. Javahiraly, M. Slaman, H. Schreuders, B. Dam, and P. Meyrueis, Opt. Express **21**, 382 (2013).
17) C. Wadell, S. Syrenova, and C. Langhammer, ACS Nano **8**, 11925 (2014).
18) C. Wadell, F. A. A. Nugroho, E. Lidström, B. Iandolo, J. B. Wagner, and C. Langhammer, Nano Lett. **15**, 3563 (2015).
19) J. Dai, L. Zhu, G. Wang, F. Xiang, Y. Qin, M. Wang, and M. Yang, Sensors **17**, 577 (2017).
20) P. Ngene, T. Radeva, M. Slaman, R. J. Westerwaal, H. Schreuders, and B. Dam, Adv. Funct. Mater. **24**, 2374 (2014).
21) J. Kukkola, J. Mäklin, N. Halonen, T. Kyllönen, G. Tóth, M. Szabó, A. Shchukarev, J.-P. Mikkola, H. Jantunen, and K. Kordás, Sens. Actuators B **153**, 293 (2011).
22) V. E. Wicke and G. H. Nernst, Ber. Bunsenges. Phys. Chem. **68**, 224 (1964).
23) M. Wilde and K. Fukutani, Surf. Sci. Rep. **69**, 196 (2014).
24) L. J. Bannenberg, H. Schreuders, L. van Eijck, J. R. Heringa, N.-J. Steinke, R. Dalgliesh, B. Dam, F. M. Mulder, and A. A. van Well, J. Phys. Chem. C **120**, 10185 (2016).
25) Z. Zhao, M. Knight, S. Kumar, E. T. Eisenbraun, and M. A. Carpenter, Sens. Actuators B **129**, 726 (2008).
26) P. Ngene, R. J. Westerwaal, S. Sachdeva, W. Haije, L. C. de Smet, and B. Dam, Angew. Chem., Int. Ed. **53**, 12081 (2014).

©2020 The Physical Society of Japan

J. Phys. Soc. Jpn.
Downloaded from journals.jps.jp by 82.161.147.56 on 11/03/20

27) F. A. A. Nugroho, I. Darmadi, L. Cusinato, A. Susarrey-Arce, H. Schreuders, L. J. Bannenberg, A. Bastos da Silva Fanta, S. Kadkhodazadeh, J. B. Wagner, T. J. Antosiewicz, A. Hellman, V. P. Zhdanov, B. Dam, and C. Langhammer, Nat. Mater. **18**, 489 (2019).
28) I. Darmadi, F. A. A. Nugroho, S. Kadkhodazadeh, J. B. Wagner, and C. Langhammer, ACS Sens. **4**, 1424 (2019).
29) C. Boelsma, L. J. Bannenberg, M. J. van Setten, N.-J. Steinke, A. A. Van Well, and B. Dam, Nat. Commun. **8**, 15718 (2017).
30) T. Mak, R. Westerwaal, M. Slaman, H. Schreuders, A. W. Van Vugt, M. Victoria, C. Boelsma, and B. Dam, Sens. Actuators B **190**, 982 (2014).
31) Y. Pivak, R. Gremaud, K. Gross, M. Gonzalez-Silveira, A. Walton, D. Book, H. Schreuders, B. Dam, and R. Griessen, Scr. Mater. **60**, 348 (2009).
32) Y. Pivak, H. Schreuders, M. Slaman, R. Griessen, and B. Dam, Int. J. Hydrogen Energy **36**, 4056 (2011).
33) R. J. Westerwaal, J. S. A. Rooijmans, L. Leclercq, D. G. Gheorghe, T. Radeva, L. Mooij, T. Mak, L. Polak, M. Slaman, B. Dam, and T. Rasing, Int. J. Hydrogen Energy **38**, 4201 (2013).
34) R. J. Westerwaal, S. Gersen, P. Ngene, H. Darmeveil, H. Schreuders, J. Middelkoop, and B. Dam, Sens. Actuators B **199**, 127 (2014).
35) L. J. Bannenberg, F. A. A. Nugroho, H. Schreuders, B. Norder, T. T. Trinh, N.-J. Steinke, A. A. van Well, C. Langhammer, and B. Dam, ACS Appl. Mater. Interfaces **11**, 15489 (2019).
36) G. C. A. M. Janssen, Thin Solid Films **515**, 6654 (2007).
37) S. Wagner and A. Pundt, Appl. Phys. Lett. **92**, 051914 (2008).
38) A. Baldi, M. Gonzalez-Silveira, V. Palmisano, B. Dam, and R. Griessen, Phys. Rev. Lett. **102**, 226102 (2009).
39) S. Wagner and A. Pundt, Int. J. Hydrogen Energy **41**, 2727 (2016).
40) A. Baldi, L. Mooij, V. Palmisano, H. Schreuders, B. Dam, B. J. Kooi, and R. Griessen, Phys. Rev. Lett. **121**, 255503 (2018).
41) R. Feenstra, G. J. de Bruin-Hordijk, H. L. M. Bakker, R. Griessen, and D. G. de Groot, J. Phys. F **13**, L13 (1983).
42) R. Gremaud, M. Slaman, H. Schreuders, B. Dam, and R. Griessen, Appl. Phys. Lett. **91**, 231916 (2007).
43) L. J. Bannenberg, C. Boelsma, H. Schreuders, S. Francke, N.-J. Steinke, A. A. Van Well, and B. Dam, Sens. Actuators B **283**, 538 (2019).
44) J. Prinz, G. K. Pálsson, P. T. Korelis, and B. Hjörvarsson, Appl. Phys. Lett. **97**, 251910 (2010).
45) F. A. A. Nugroho, I. Darmadi, V. P. Zhdanov, and C. Langhammer, ACS Nano **12**, 9903 (2018).
46) K. Palm, J. Murray, T. C. Narayan, and J. N. Munday, ACS Photonics **5**, 4677 (2018).
47) K. J. Palm, J. B. Murray, J. P. McClure, M. S. Leite, and J. N. Munday, ACS Appl. Mater. Interfaces **11**, 45057 (2019).
48) N. A. Isaac, P. Ngene, R. J. Westerwaal, J. Gaury, B. Dam, A. Schmidt-Ott, and G. Biskos, Sens. Actuators B **221**, 290 (2015).
49) M. Wang and Y. Feng, Sens. Actuators B **123**, 101 (2007).
50) R. J. Westerwaal, N. Duim, I. Nieuwenhuijse, C. Perrotton, A. Dabirian, J. M. van Leeuwen, V. Palmisano, and B. Dam, Sens. Actuators B **165**, 88 (2012).
51) M. Slaman, B. Dam, M. Pasturel, D. M. Borsa, H. Schreuders, J. Rector, and R. Griessen, Sens. Actuators B **123**, 538 (2007).
52) R. Gremaud, J. L. M. Van Mechelen, H. Schreuders, M. Slaman, B. Dam, and R. Griessen, Int. J. Hydrogen Energy **34**, 8951 (2009).
53) V. Palmisano, M. Filippi, A. Baldi, M. Slaman, H. Schreuders, and B. Dam, Int. J. Hydrogen Energy **35**, 12574 (2010).
54) M. Victoria, R. J. Westerwaal, B. Dam, and J. L. M. van Mechelen, ACS Sens. **1**, 222 (2016).
55) C. Boelsma, Dr. Thesis, Delft University of Technology (2017).
56) T. Radeva, P. Ngene, M. Slaman, R. Westerwaal, H. Schreuders, and B. Dam, Sens. Actuators B **203**, 745 (2014).
57) P. Ngene, A. Longo, L. Mooij, W. Bras, and B. Dam, Nat. Commun. **8**, 1846 (2017).
58) L. P. A. Mooij, A. Baldi, C. Boelsma, K. Shen, M. Wagemaker, Y. Pivak, H. Schreuders, R. Griessen, and B. Dam, Adv. Energy Mater. **1**, 754 (2011).
59) A. San-Martin and F. D. Manchester, J. Phase Equilibria **12**, 332 (1991).
60) T. Schober, Solid State Phenom. **49–50**, 357 (1996).
61) M. H. Mintz, Solid State Phenom. **49–50**, 331 (1996).

Lars Bannenberg received his master in Applied Physics from Delft University of Technology as well as his master in Financial Economics from Erasmus University Rotterdam in 2015. He joined the Faculty of Applied Sciences of Delft University of Technology as a Ph.D. candidate where he obtained his Ph.D. in 2019 with the thesis entitled "Skyrmions and Spirals in Cubic Chiral Magnets". In his research, he applies a wide range of neutron scattering techniques. In addition, he continued his work on thin film metal hydrides in corporation with the Materials for Energy Conversion and Storage (MECS) group in the department of Chemical Engineering as well as his study of initial public offers at the Erasmus University of Rotterdam.

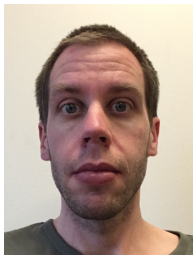

Christiaan Boelsma received his master in condensed matter physics in 2011. He performed his master thesis (titled: "Enthalpy-Entropy Compensation in Metal Hydrides") in the Condensed Matter Group of the Physics Department of the Vrije Universiteit in Amsterdam. He continued his work in the field of metal hydrides in the MECS group at the Delft University of Technology, where he also obtained his Ph.D. in 2017 with his thesis entitled "Tailoring the Hydrogen Detection Properties of Metal Hydrides".

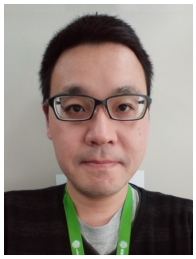

Kohta Asano received his Ph.D. at Tohoku University in 2005 for a thesis on the hydrogen absorption and desorption processes of $LaNi_5$ based alloys. He joined the National Institute of Advanced Industrial Science and Technology (AIST) in Tsukuba and started to study the diffusion of hydrogen in metals using solid state NMR and the synthesis of novel Mg based alloys and hydrides. He also studied metal hydride thin films in the MECS group at Delft University of Technology from 2013 to 2014 under the Researcher Exchange Program between the Japan Society for the Promotion of Science (JSPS) and the Netherlands Organization for Scientific Research (NWO).

Herman Schreuders received his bachelor in engineering physics from the Hogeschool Rijswijk. In 1995 he joined Philips Research in Eindhoven, The Netherlands. Within Philips he researched cathode ray tubes, liquid crystal displays and plasma displays. In 2003, he started as an engineer in the Condensed Matter Physics Group of the Vrije Universiteit in Amsterdam. Main responsibilities included sputter deposition of thin films for projects within the group. In 2009 the hydrogen research moved to the MECS group in the department Chemical Engineering at Delft University of Technology where he continued the work on hydrogen sensors, switchable mirrors and lightweight hydrogen storage materials.

Bernard Dam received his Ph.D. at the Radboud University Nijmegen in 1986 for a thesis on the growth and morphology of incommensurate crystals. At Philips Research Labs Eindhoven he investigated the growth of thin film high-T_C superconductors and other functional complex oxides. In 1992 he joined the Condensed Matter Department of the Vrije Universiteit Amsterdam in the group of Professor R. Griessen. After studying defect pinning in high-T_C superconductors, he turned to the field of metal hydrides. He developed a research line focusing on the application of metal hydrides for sustainable energy applications, including hydrogen storage, sensors, membranes, etc., using a thin film combinatorial approach. Since 2009, he is the head of the MECS group at the Department of Chemical Engineering at Delft University of Technology. In addition to the metal hydride research, his group specializes in electrochemical conversion processes and the properties of oxyhydrides.

©2020 The Physical Society of Japan